Influence of ENSO on Flood Frequency along the California Coast

E. D. ANDREWS AND RONALD C. ANTWEILER

U.S. Geological Survey/WRD, Boulder, Colorado

PAUL J. NEIMAN AND F. MARTIN RALPH

NOAA/Environmental Technology Laboratory, Boulder, Colorado

ABSTRACT

The influence of the El Niño–Southern Oscillation (ENSO) phenomenon on flooding in California coastal streams is investigated by analyzing the annual peak floods recorded at 38 gauging stations. The state of ENSO prior to and during flooding is characterized by the multivariate ENSO index (MEI), where MEI < -0.5 is defined as the La Niña phase and MEI > 0.5 as the El Niño phase. Flood magnitude in all 20 streams located south of 35°N has a significant positive correlation ($r = 0.3$ to 0.6), whereas in 3 of the 4 streams located north of 41°N flood magnitude has a significant negative correlation ($r = -0.3$ to -0.4), with MEI from -2.2 to $+3.2$. Correlations with MEI are uniformly weak and insignificant, however, when the floods are subdivided into El Niño and non–El Niño phases. A comparison of the geometric mean El Niño flood to the geometric mean non–El Niño flood determined that the means were statistically different at gauging stations south of 35°N and north of 41°N. For 20 streams located south of 35°N, the geometric mean of annual peak floods recorded at a stream gauge during El Niño phases is 2–14 times the geometric mean of annual peak floods recorded during non–El Niño phases. Thus, south of 35°N along the California coast, floods are significantly larger during an El Niño phase than a non–El Niño phase. For the three streams located north of 41°N, the geometric mean of annual peak floods during an El Niño phase was less than 70% of the geometric mean of annual peak floods during a non–El Niño phase. The relative strength of the El Niño phase, however, has, at most, a weak influence on flood magnitude. Flood exceedance probabilities for the El Niño and non–El Niño periods were calculated for all gauging stations using a three-parameter log gamma distribution. For exceedance probabilities from 0.50 to 0.02, the ratio of the El Niño to non–El Niño floods varies from greater than 10 near 32°N to less than 0.7 near 42°N. Latitude explains 76%–90% of the observed variation in the relative magnitude of El Niño versus non–El Niño floods over the range of exceedance probabilities.

1. Introduction

Recently, the connection between El Niño–Southern Oscillation (ENSO) and climate across western North America has been of considerable scientific interest. Many investigations have explored various aspects of this connection, including its relation to anomalous precipitation (e.g., Ropelewski and Halpert 1986; Schonher and Nicholson 1989; Redmond and Koch 1991; Livezey et al. 1997; Dettinger et al. 1998, 2000), and streamflow (Cayan and Peterson 1989; Cayan and Webb 1992; Kahya and Dracup 1994; Dracup and Kahya 1994; Mitchell and Blier 1997; Cayan et al. 1999; Higgins et al. 2000). The several studies have produced rather disparate results. Some of the differences, no doubt, are a result of the various temporal and spatial scales at which the questions have been considered. A general consensus,

however, appears to have emerged over the past decade. Most, if not all, studies have concluded that the connection of precipitation and streamflows to ENSO varies greatly across the state of California, south to north and from the coast to inland (e.g., Schonher and Nicholson 1989; Redmond and Koch 1991; Webb and Betancourt 1992; Cayan et al. 1999). This study focuses on coastal streams because wintertime precipitation in the coastal mountains is more sensitive to the phase of ENSO than the interior (e.g., Schonher and Nicholson 1989) and because the hydrometeorologic complexity increases inland (e.g., Cayan and Peterson 1989; Cayan and Webb 1992; Ely et al. 1994).

Schonher and Nicholson (1989) concluded that annual precipitation was above average statewide during El Niño episodes between 1951 and 1978, and during the winter of 1982/83. Excess precipitation was greatest in the south, 160%–185% of the mean, and decreased northward to only 120%–125% of the mean in northern California. Eight of the 10 wettest years and none of the 10 driest years in coastal southern California were

Corresponding author address: Dr. E. D. Andrews, U.S. Geological Survey/WRD, 3215 Marine St., Suite E127, Boulder, CO 80303.
E-mail: eandrews@usgs.gov

El Niño years, whereas 5 of the 10 wettest years and 3 of the 10 driest years in coastal northern California were El Niño years. Annual precipitation on coastal central California was intermediate.

Redmond and Koch (1991) investigated the correlation between October/March precipitation and the mean Southern Oscillation index (SOI) for the preceding June–November. All of coastal California tended to receive increased precipitation during El Niño–like conditions and decreased precipitation during La Niña conditions. Correlations were strongest in the south and decreased northward along the coast to the border with Oregon. Only the correlations within coastal southern California were significant.

Cayan et al. (1999) investigated the frequency with which daily precipitation and streamflow across the western United States exceeded the 50th and 90th percentile value in relation to the SOI. The frequency of 90th percentile precipitation and streamflow was greatly enhanced across coastal southern California during the El Niño phase versus the La Niña phase. The relative enhancement diminished northward and vanished along coastal northern California. These results are quite significant. They demonstrate that relatively infrequent daily precipitation and streamflows were enhanced over a similar geographical region as previously shown for seasonal and annual precipitation. Annual peak floods, however, are considerably larger than the 90th percentile daily mean flow in California coastal streams. For example, south of 35°N, the annual peak flood with a 5-yr recurrence interval is typically greater than 100 times the 90th percentile daily mean flow. The difference decreases northward, however, the 5-yr flood is still 10 times the 90th percentile daily mean flow in drainage basins north of 40°N.

This investigation is part of a comprehensive examination of the magnitude and frequency of erosion in California coastal watersheds. The purpose of the investigation was to extend our understanding of the connection between ENSO phase and hydrology to the most infrequent, large streamflows that are a major natural hazard. Estimated flood-related damage during the 1995 El Niño was approximately \$3.3 billion (Ross and Lott 2000). The significance of these floods is not limited to inundation of the riparian zone: they are also responsible for transporting a large portion of the sediment eroded from these watersheds (Inman and Jenkins 1999). An analysis of sediment transport in the Ventura River, north and west of Los Angeles, found that 98% of all sediment transported during the 72-yr period from 1929 to 2000 was carried by the 81 days of largest flow. Streamflows that are equaled or exceeded approximately 1 day yr^{-1} or less on average are those that erode, transport, and deposit the vast majority of all sediment in the coastal watersheds. This study examines how ENSO phase influences the magnitude of flooding in California coastal streams.

2. Historical record of annual peak floods

All gauging station records collected on streams draining the seaward flank of the California coast range were examined to identify those which were operated during the period 1950–2000 and were relatively unaffected by flow regulation. The 38 gauging stations selected for this study are identified and their locations are shown in Fig. 1. The gauging station identification numbers and drainage areas are listed in Table 1. The period of record considered, 1950–2000, was determined by the length of the available streamflow records. In order to obtain a relatively dense geographical coverage along the California coast, some gauging stations that were not operated continuously over the entire period 1950–2000 have been included in this study. Nine of the gauging stations shown in Table 1 have less than 48 yr of records, while only San Antonio Creek near Lockwood (1965–2000) and Nacimiento River below Sapaque Creek near Bryson (1971–2000), have less than 40 yr of record.

Most of the gauging stations are located within 20 km of the coast and several are within a few kilometers. The main-stem channel upstream of each gauge is shown in Fig. 1 to indicate the general aspect of the contributing drainage basin. Many of the basins are oriented so that they lie on the windward slopes for storms moving onshore from the southwest quarter.

The multivariate ENSO index (MEI) developed by Wolter and Timlin (1993, 1998) was applied to characterize the ENSO phase during and prior to each of the recorded annual peak floods. The MEI is calculated from an analysis of sea level pressure, zonal and meridional wind components, sea surface and air temperature, and the total cloudiness recorded over the tropical Pacific region. The index is computed every month using information recorded during the preceding two months. (The MEI time series is available online at http://www.cdc.noaa.gov/~kew/MEI.) A positive value indicates an El Niño–like condition, while a negative value indicates a La Niña–like condition. Approximately one-third of the monthly values since 1950 are greater than +0.5 and indicate a developed El Niño condition. Similarly, approximately one-third of the monthly values are less than −0.5 and indicate a developed La Niña condition. Annual peak floods are identified to have occurred during an El Niño, neutral, or La Niña phase based on the coincident MEI. For the majority of the gauging stations with a continuous record of annual peak floods, 1950–2000, 16 of the floods occurred during an El Niño phase and 35 floods occurred during a neutral or La Niña phase.

Eighty-seven percent of all annual peak floods recorded at the 38 gauging stations studied occurred during the months of December/March, the period of greatest rainfall along the California coast. Although snowfall can occur occasionally in the coastal watersheds, annual peak floods in the basins selected for this analysis
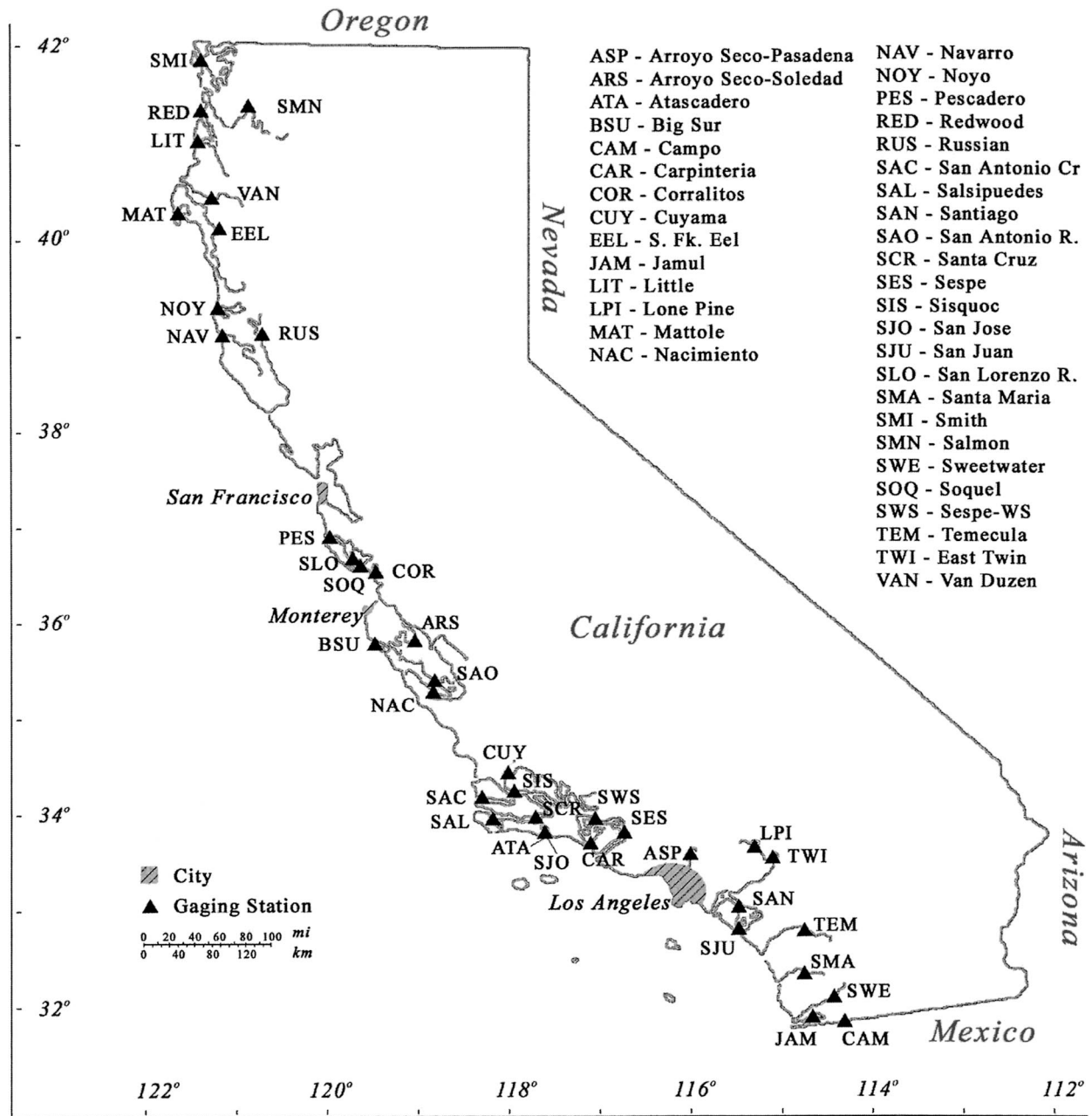
FIG. 1. Location of gauging stations with recorded annual peak floods.

are overwhelmingly the immediate result of heavy rainfall. Fu et al. (1986) proposed a classification of El Niño episodes. The Type-I ENSO pattern consists of anomalously warm sea surface temperatures extending far east of the international date line, which persist well through the winter months. Given the way in which El Niño floods are identified for this study (i.e., no lag) and that they have occurred with few exceptions during the November/March period, they fall within Fu's Type-I El Niño category.

3. Correlation of annual peak floods with ENSO

As previously noted, Cayan and Peterson (1989) found a significant correlation of monthly mean streamflow with ENSO phase in the western United States. Monthly mean streamflow increased with El Niño strength from southern California throughout the Southwest and decreased with strengthened La Niña conditions, while an opposite response to ENSO phase was found in the Pacific Northwest. Redmond and Koch (1991) found generally similar correlations between
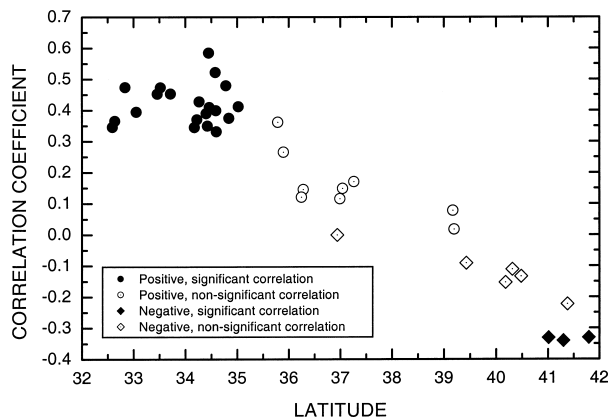
TABLE 1. Computed flood magnitude for specified recurrence intervals during El Niño (MEI > 0.5) and non–El Niño (MEI < 0.5) periods at selected streamflow gauging stations along the California coast.

USGS station No.	Gauging station name	Station code	Basin area (km^2)	El Niño (MEI > 0.5)			Non–El Niño (MEI < 0.5)		
				5 yr m^3 s^{-1}	10 yr m^3 s^{-1}	50 yr m^3 s^{-1}	5 yr m^3 s^{-1}	10 yr m^3 s^{-1}	50 yr m^3 s^{-1}
11532500	Smith River near Crescent City	SMI	1589	2900	3300	4300	3800	4400	5900
11522500	Salmon River at Somes Bar	SMN	1945	840	1000	1400	1300	1700	3000
11482500	Redwood Creek at Orick	RED	717	740	920	1300	1000	1300	1800
11481200	Little River near Trinidad	LIT	105	170	210	300	230	280	390
11478500	Van Duzen River near Bridgeville	VAN	575	930	1100	1500	860	1000	1300
11469000	Mattole River near Petrolia	MAT	635	1400	1700	2300	1500	1800	2500
11476500	South Fork Eel River near Miranda	EEL	1391	2100	2400	3000	2500	3400	5600
11468500	Noyo River near Fort Bragg	NOY	275	330	430	630	340	460	810
11461000	Russian River near Ukiah	RUS	259	370	430	550	330	410	610
11468000	Navarro River near Navarro	NAV	785	990	1200	1700	920	1300	2400
11162500	Pescadero Creek near Pescadero	PES	119	160	240	450	110	160	310
11160500	San Lorenzo River at Big Trees	SLO	275	420	600	1100	300	420	770
11160000	Soquel Creek at Soquel	SOQ	104	130	170	260	150	230	450
11159200	Corralitos Creek at Freedom	COR	72	59	79	130	74	130	340
11152000	Arroyo Seco near Soledad	ARS	632	580	780	1200	380	530	940
11149900	San Antonio River near Lockwood	SAO	603	440	690	1400	230	430	1300
11148900	Nacimiento River near Bryson	NAC	420	1440	2100	3800	580	880	1800
11143000	Big Sur River near Big Sur	BSU	120	160	210	310	110	140	240
11136800	Cuyama River near Santa Maria	CUY	2295	420	790	2200	72	160	670
11138500	Sisquoc River near Sisquoc	SIS	728	310	420	680	75	130	310
11136100	San Antonio Creek near Casmalia	SAC	350	74	130	320	14	24	62
11124500	Santa Cruz Creek near Santa Ynez	SCR	192	130	160	230	45	70	150
11132500	Salsipuedes Creek near Lompoc	SAL	122	190	230	310	95	160	390
11111500	Sespe Creek near Wheeler Springs	SWS	128	250	410	880	47	95	320
11113000	Sespe Creek near Fillmore	SES	650	1800	2200	3000	340	550	1300
11120500	San Jose Creek near Goleta	SJO	14	47	69	130	17	25	48
11120000	Atascadero Creek near Goleta	ATA	49	180	280	590	51	77	160
11119500	Carpinteria Creek near Carpinteria	CAR	3	85	160	440	31	57	170
11063500	Lone Pine Creek near Keenbrook	LPI	39	29	41	74	6.6	11	27
11098000	Arroyo Seco near Pasadena	ASP	41	120	180	360	26	39	84
11058500	East Twin Creek near Arrowhead Springs	TWI	23	47	78	170	12	21	56
11075800	Santiago Creek at Modjeska	SAN	34	86	130	270	16	31	90
11046530	San Juan Creek at San Juan Capistrano	SJU	282	340	670	1900	34	80	340
11042400	Temecula Creek near Aguanga	TEM	339	71	110	220	20	36	100
11028500	Santa Maria Creek near Ramona	SMA	149	120	190	390	8.2	19	84
11015000	Sweetwater River near Descanso	SWE	118	78	180	720	12	26	110
11014000	Jamul Creek near Jamul	JAM	182	86	160	440	11	24	99
11012500	Campo Creek near Campo	CAM	220	12	35	180	2.4	7.2	51

ENSO and mean October/March precipitation in the western United States. Both studies found the largest correlations occurred when the hydrologic response lagged the ENSO phase by several months. Correlations between ENSO phase and monthly mean streamflow were found to be generally weak and not significant along the central and northern California coast.

The distribution of annual peak floods at a gauging station is typically nonnormal and fails to meet the assumptions required for a parametric statistical analysis. The normality requirement, however, can be met by using the log-transformed flood discharges. Accordingly, the log-transformed annual peak floods, log Q_{pk}, were correlated with the MEI using various lags for all 38 gauging station records. The best correlations were obtained using the coincident MEI values (i.e., no lag), although for some records the correlation of log Q_{pk} with the MEI values was nearly as good 1–6 months prior to the flood.

Correlation coefficients calculated for the regression of log Q_{pk} on the coincident MEI are plotted versus latitude in Fig. 2. Annual peak floods recorded at the 20 gauges located south of 35°N have a significant positive correlation with the coincident MEI. Annual flood discharges recorded in drainage basins between 35° and 40°N have no significant correlation with MEI. North of 41°N, the log Q_{pk}s recorded at three stream gauges have a significant negative correlation with MEI.

The results summarized in Fig. 2 exhibit a well-defined trend with latitude in the correlation of log Q_{pk} with MEI. The broad geographical pattern is consistent with the variations in seasonal precipitation (Schonher and Nicholson 1986; Redmond and Koch 1991) and streamflow (Cayan and Peterson 1989; Cayan et al.

FIG. 2. Variation in correlation coefficient of log flood discharge on MEI vs gauge latitude.
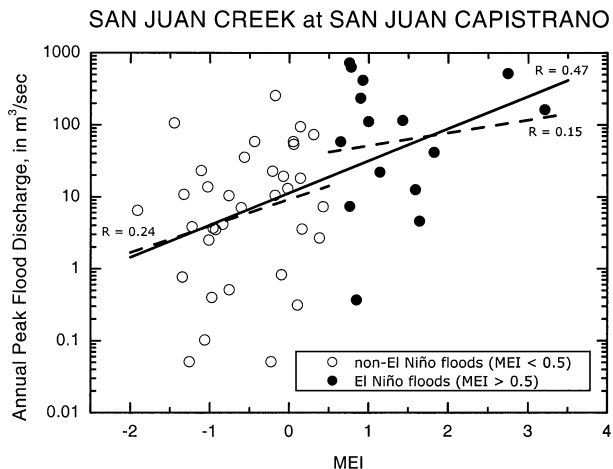
SAN JUAN CREEK at SAN JUAN CAPISTRANO

FIG. 3. Correlation of annual peak flood vs concurrent MEI at the San Juan Creek near the San Juan Capistrano gauge.

1999) over the range of ENSO conditions. There are also notable differences between prior studies and these results. Previous studies have found little or no correlation between monthly mean and seasonal precipitation and streamflow along the California coast north of 37°N. Our analysis shows that annual peak floods have a significant negative correlation with ENSO phase much farther south, near 41°N, than appears to occur with either monthly mean and seasonal precipitation and streamflow.

The correlations of log Q_{pk} with MEI, even for those 20 gauges located south of 35°N, $r = 0.3$ to 0.6, are not especially strong. In fact, when the analysis is repeated after separating the floods into two subsamples—those annual peak floods that occurred when El Niño conditions prevailed (MEI $\geq$ 0.5) and those annual peak floods that occurred when non–El Niño conditions prevailed (MEI $<$ 0.5)—no significant correlation between flood magnitude and MEI was found at any gauging station. For example, annual peak floods recorded at the San Juan Creek at San Juan Capistrano are plotted versus MEI in Fig. 3. The correlation coefficient for all floods recorded at this gauge is 0.47 and highly significant. In contrast, the correlation coefficient of only the El Niño floods with MEI is 0.15 and is not significant. The correlation coefficient of only the non–El Niño floods with MEI is 0.24 and is not significant. As shown in Fig. 3, four of the five largest annual peak floods recorded at the San Juan Creek gauge have occurred during a weakly developed El Niño phase, $0.5 < $ MEI < 1.0.

The result of this analysis is the same for all 20 gauging stations located south of 35°N. When annual peak floods are segregated into El Niño and non–El Niño subsamples, correlation coefficients are only one-half to one-quarter of the value for the whole population and none of the correlation coefficients were found to be significant for either subsamples at any gauge. Thus, rather than a linear relation of flood magnitude with MEI (La Niña to El Niño), annual floods recorded at

the 20 gauging stations located south of 35°N appear to consist of two populations. Similarly, the significant negative correlation of flood magnitude with MEI calculated for three gauges located north of 41°N vanishes when the analysis is repeated using the El Niño and non–El Niño subsamples.

Accordingly, annual peak floods recorded at all gauging stations considered in this study were separated into an El Niño population, MEI $\geq$ 0.5 and a non–El Niño population, MEI $<$ 0.5. The first objective of the analysis is to compare the two subsample geometric means, determine whether the differences are significant, and identify any geographical trends in the means. As noted above, flood discharges were log transformed in order to normalize the populations. The ratio of the geometric means of the El Niño and non–El Niño floods, that is,

$$\frac{\overline{\log Q_{pk}(\text{El Niño})}}{\overline{\log Q_{pk}(\text{non–El Niño})}}, \tag{1}$$

is plotted versus gauging station latitude in Fig. 4. The south–north trend in the ratio of geometric mean flood during El Niño and non–El Niño periods shown in Fig. 4 is broadly similar to the south–north trend in the correlation of flood magnitude with MEI previously described in Fig. 2. The ratio of the geometric mean El Niño flood to the geometric mean non–El Niño flood is large in southern California coastal streams and decreases northward. The average ratio for the seven gauging stations located south of 34°N is 6.7, with a maximum of 14. Northward of 41°N, the ratio is less than 0.70, with a minimum value of 0.65 in the Salmon River at Somes Bar.

The analysis also considered whether the geometric mean of annual peak floods during neutral ENSO phases, $0.5 > $ MEI $ > -0.5$ was different from the geometric mean of annual peak floods during La Niña phases. Only three gauging stations, all south of 34°N, had statistically significant larger geometric means during neutral
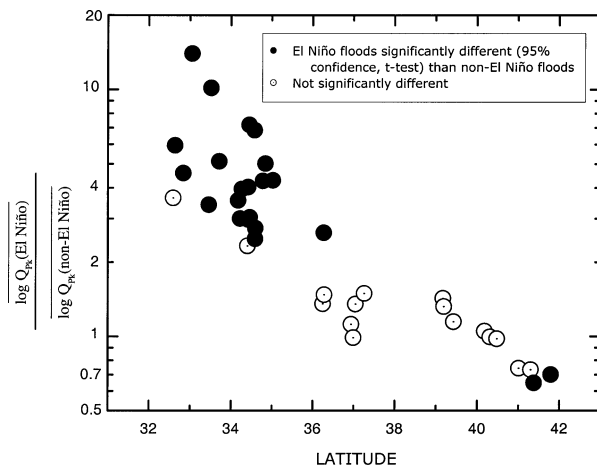
FIG. 4. Variation in the ratio of geometric mean El Niño flood to geometric mean non–El Niño flood vs gauge station latitude.

ENSO phases than La Niña phases. Other nearby gauging stations, also south of 34°N, however, did not have significantly different geometric means during neutral ENSO and La Niña phases. When the results of the significance tests are adjusted for the total number of gauging stations considered (38), none of the flood records have significantly different geometric means of annual peak floods during neutral ENSO and La Niña phases. Therefore, two subsamples, El Niño (MEI $\geq$ 0.5) and non–El Niño (MEI $<$ 0.5), are considered in the subsequent analysis. Webb and Betancourt (1992) found the same distinction in their analysis of variations in flood magnitude with ENSO phase in the Santa Cruz River of southern Arizona. Annual peak floods during an El Niño phase tended to be larger than annual peak floods during neutral and La Niña phases. There was, however, no difference in flood magnitude between the neutral and La Niña phases.

4. Analysis of flood frequency

a. Variation with latitude

The common method for flood frequency analysis in the United States employs a three-parameter log-gamma distribution (commonly known as log-Pearson Type III in the hydrological literature) and is described in Bulletin 17B, prepared by the U.S. Water Resources Council (1982). Fitting a log gamma distribution to the observed series of annual peak discharges recorded at a gauging station entails estimating the mean, standard deviation, and skew of the log-transformed values. Given sufficient length of record, estimates for the mean and standard deviation are calculated from the observed gauging station record. Gauging station records, however, are generally too short to calculate a reliable estimate of the distribution skew. Consequently, the method described in Bulletin 17B relies on a regional estimate of the flood population skew at a gauging station.

Exceedance probabilities of floods during an El Niño phase, MEI $>$ 0.5 were calculated for the 38 gauging stations in this study by fitting a three-parameter log gamma distribution. Each gauging station record was separated into an El Niño and non–El Niño subsample based upon the coincident MEI value. A mean and standard deviation of the subsample log Q_{pk} were calculated for each subsample. Because the regional skew estimates described in Bulletin 17B were calculated for whole records rather than separately for El Niño and non–El Niño subsamples, the available regional skew values could not be used for this analysis. Instead, skew values of the El Niño and non–El Niño subsamples were calculated for each gauging station record. Neither the El Niño nor the non–El Niño skews show any trend with the basin location along the coast. The mean skew of all El Niño subsamples is -0.45, whereas the mean skew of all non–El Niño subsamples is -0.05. These two skew values are statistically different. Accordingly, the exceedance probabilities for floods during El Niño periods were calculated using a skew of -0.45, whereas a skew of -0.05 was assumed for the non–El Niño periods.

Many of the streams considered in this analysis, particularly those with smaller drainage areas in the more arid parts of the state, do not have a flood, that is, direct storm runoff, every year. In some instances, there was little or no recorded flow during an entire year. For example, there have been 9 yr when the annual maximum streamflow recorded at the Santa Maria Creek near Ramona has been less than 0.03 m^3 s^{-1}. The computed flood frequency at a gauge can vary substantially with the inclusion or exclusion of one or two unusually small annual maximum streamflows. The identification of what constitutes an unusually small annual maximum streamflow is somewhat subjective and a variety of criteria have been proposed. A common criteria in flood frequency analysis, and the one we have adopted for this study, is to reject values at the 1% level of significance in a one-sided test.

Flood magnitudes calculated for the 0.20, 0.10, and 0.02 exceedance probabilities during El Niño and non–El Niño phases at all 38 gauging stations used in this analysis are listed in Table 1. Differences in the calculated magnitude of El Niño and non–El Niño floods are primarily due to the differences in the mean log Q_{pk} of the subsample, as summarized in Fig. 4. Standard deviations of log Q_{pk} calculated for the El Niño and non–El Niño subsamples were not significantly different. Interestingly, this result is the converse of that found by Webb and Betancourt (1992) in the analysis of El Niño and non–El Niño floods in the Santa Cruz River of southern Arizona. They determined that the mean El Niño and non–El Niño floods were not significantly different, whereas subsample standard deviations were different. Santa Cruz River flood hydrology, however, is not directly comparable to California coastal streams because of the importance of dissipating tropical cy-
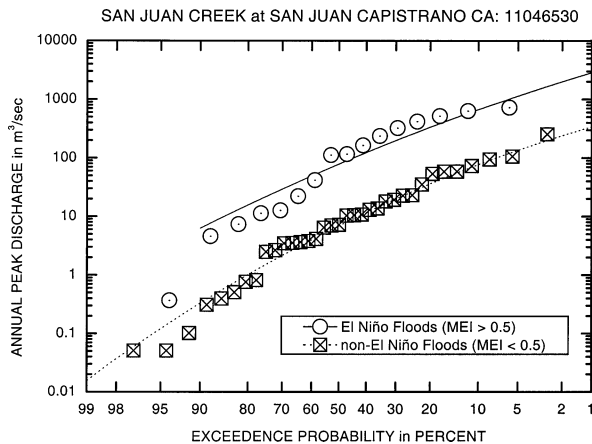
FIG. 5. Comparison of observed El Niño and non–El Niño annual peak floods with fitted three-parameter log gamma distribution computed for San Juan Creek at San Juan Capistrano. Gauge location is identified as SJU in Fig. 1.
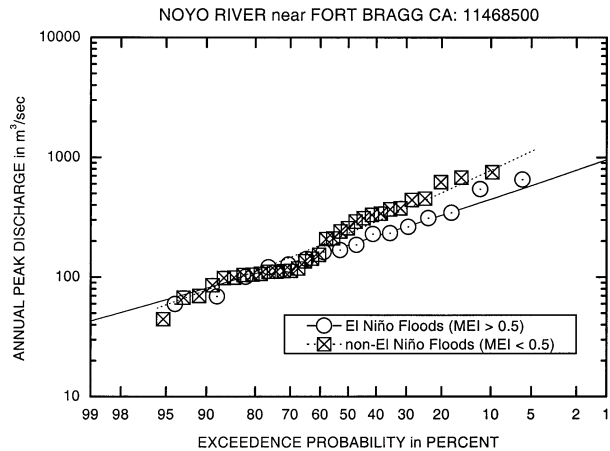

FIG. 6. Comparison of observed El Niño and non–El Niño annual peak floods with fitted three-parameter log gamma distribution computed for the Noyo River near Fort Bragg. Gauge location is identified as NOY in Fig. 1.

clones and summer monsoonal storms in Arizona (Cayan and Webb 1992).

Flood magnitudes for various exceedance probabilities calculated for El Niño and non–El Niño periods at the San Juan Creek at the San Juan Capistrano gauging station are compared in Fig. 5. San Juan Creek is one of the southernmost drainage basins in this study and is representative of those streams where the geometric mean El Niño flood greatly exceeds the geometric mean non–El Niño flood (see Fig. 4). Since 1950, 16 of the annual peak floods have occurred during an El Niño, whereas 35 of the annual peak floods have occurred during a non–El Niño. The five largest annual peaks recorded since 1950 have all occurred during El Niños. One unusually small annual maximum instantaneous flow was identified in the El Niño subsample and was excluded from the calculation of flood exceedance probabilities as indicated by the length of the fitted line. At an exceedance probability of 20% ($p_e = 0.20$) the El Niño flood, $Q_{pk} = 340$ m^3 s^{-1} is approximately 10 times the corresponding non–El Niño flood, $Q_{pk} = 34$ m^3 s^{-1}. At an exceedance probability of 2%, the El Niño flood is 1900 compared to 340 m^3 s^{-1} for the non–El Niño flood. The decreasing ratio between the El Niño and non–El Niño floods with decreasing exceedance probability is a direct consequence of using a more negative skew when fitting the El Niño subsample.

Flood magnitudes calculated for a range of exceedance probabilities for El Niño and non–El Niño phases at the Noyo River near Fort Bragg gauge are compared in Fig. 6. The Noyo River basin is located northwest of San Francisco. The Noyo River, together with the nearby Navarro River near Navarro and the Russian River near Ukiah are the streams where the El Niño and non–El Niño annual peak floods appear to be nearly identical over a wide range of exceedance probabilities. Since 1952, 16 of the annual peaks have occurred during an El Niño, whereas 33 of the annual peaks have occurred

during a non–El Niño. Only two of the nine largest annual peak floods have occurred during an El Niño. For the 20% exceedance probability, the El Niño flood is 330 compared to 340 m^3 s^{-1} for the non–El Niño flood. To the south of these streams, El Niño annual peak floods exceed non–El Niño floods over a wide range of exceedance probabilities (see Table 1) at all except two gauges, Soquel Creek at Soquel and Corralitos Creek at Freedom. The explanation for these exceptions will be discussed later in this section. Northward from the Noyo River, El Niño annual peak floods are smaller than non–El Niño floods over a wide range of exceedance probabilities at all except one gauge, the Van Duzen River near Bridgeville.

Annual peak flood magnitudes calculated for a range of exceedance probabilities for El Niño and non–El Niño periods at the Salmon River at Somes Bar gauge are compared in Fig. 7. Since 1950, 18 annual peaks have occurred during an El Niño, whereas 33 annual peaks have occurred during a non–El Niño. The 11 largest annual peak floods have all occurred while non–El Niño conditions prevailed. The magnitude of El Niño annual peak floods is approximately 60% of the corresponding non–El Niño floods.

Figures 5–7 illustrate a south–north trend of decreasing flood magnitude during El Niño phases relative to non–El Niño phases. This trend is summarized in Fig. 8a for the $p_e = 0.20$ floods and Fig. 8b for the $p_e = 0.02$ floods. The ordinate value, R_q, in Figs. 8a and 8b was calculated as the ratio

$$R_q = \frac{2Q_{el}(p_e)}{Q_{el}(p_e) + Q_n(p_e)}, \qquad (2)$$

which is a normalized measure of the relative magnitude of the El Niño annual peak floods, Q_{el}, versus non–El Niño annual peak floods, Q_n. The ratio, R_q, is bounded such that when $Q_{el}(p_e) \gg Q_n(p_e)$, the ratio approaches

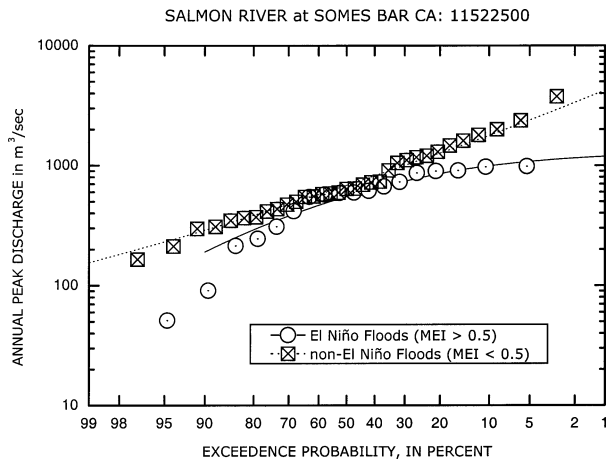SALMON RIVER at SOMES BAR CA: 11522500

FIG. 7. Comparison of observed El Niño and non–El Niño annual peak floods with fitted three-parameter log gamma distribution computed for Salmon River at Somes Bar. Gauge location is identified as SMN in Fig. 1.

2. Conversely, when $Q_{el}(p_e) \ll Q_n(p_e)$, the ratio approaches 0. Latitude explains 90% of the variation in the relative magnitude of El Niño annual peak floods at $p_e = 0.20$ and 76% of the variation in the relative magnitude of El Niño annual peak floods at $p_e = 0.02$. Values for Soquel Creek and Corralitos Creek are plotted in Figs. 8a and 8b; however, they are distinct outliers and were excluded from the correlation analysis.

b. Sensitivity of rain shadow location to ENSO phase

The north–south variation in flood magnitude along the California coast during El Niño and non–El Niño phases is a direct consequence of the location of the polar jet relative to the coastline. Several studies (e.g., Rasmusson 1985; Cayan and Webb 1992; Livezey et al. 1997) have described the eastward extension and southward displacement of the polar jet during the November–March period when El Niño conditions prevail. As a result, the polar jet that transports moisture from the tropical east Pacific intersects the California coast on average farther south during an El Niño phase than a non–El Niño phase. The eastward extension and southern displacement of the wintertime polar jet appears to explain most of the north–south trend in the relative magnitude of flooding during El Niño and non–El Niño phases.

In addition to the frequent southward displacement of the wintertime polar jet along California during the El Niño phase, the jet is typically rotated so that flow is more meridional, southerly, compared to the La Niña phase when the jet tends to be more zonal, westerly (e.g., Rasmusson and Wallace 1983; Webb and Betancourt 1992). Depending on the topography south and west of a given drainage basin, relative rotation of the polar jet between the El Niño and La Niña phases can substantially affect storm precipitation and flood mag-
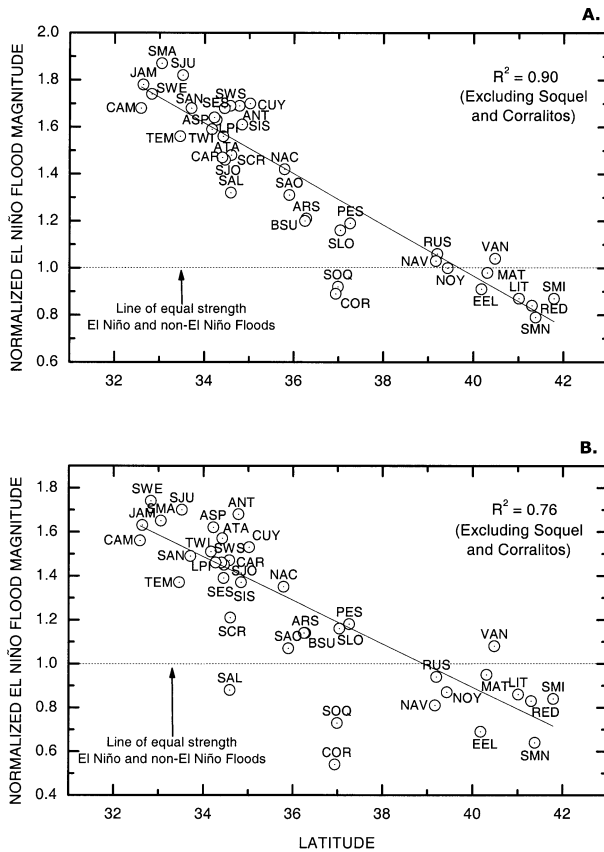
FIG. 8. Variation in the relative magnitude of normalized El Niño annual peak floods computed for two exceedance probabilities: (a) $p_e = 0.20$ and (b) $p_e = 0.02$.

nitude. As noted above, the annual floods recorded at two gauges, Soquel Creek at Soquel and Corralitos Creek at Freedom, deviate significantly from the north–south pattern followed by other gauges along the California coast. They are the only gauges studied south of the Noyo River near Fort Bragg, where the El Niño floods are less than the non–El Niño floods over all exceedance probabilities. The $p_e = 0.20$ El Niño flood of Corralitos Creek is less than 60% of the magnitude one would expect given the basin latitude. The following analysis shows that the anomalously small ratio of El Niño to non–El Niño floods in the Soquel and Corralitos basins is the result of a rain shadow over these basins created by the Santa Lucia Mountains when the prevailing wind direction is predominantly from the south.

Figure 9 shows a portion of the California coast centered around the Santa Lucia Mountains. The location of the eight gauging stations analyzed in this study within this area, including the Soquel Creek and Corralitos Creek gauges are shown. The extent of the Santa Lucia Mountains is indicated by the shaded relief. Beside the gauge station symbol at each location, the relative magnitude of the $p_e = 0.20$ El Niño flood, R_q, is shown. These are the same values plotted in Fig. 8a.

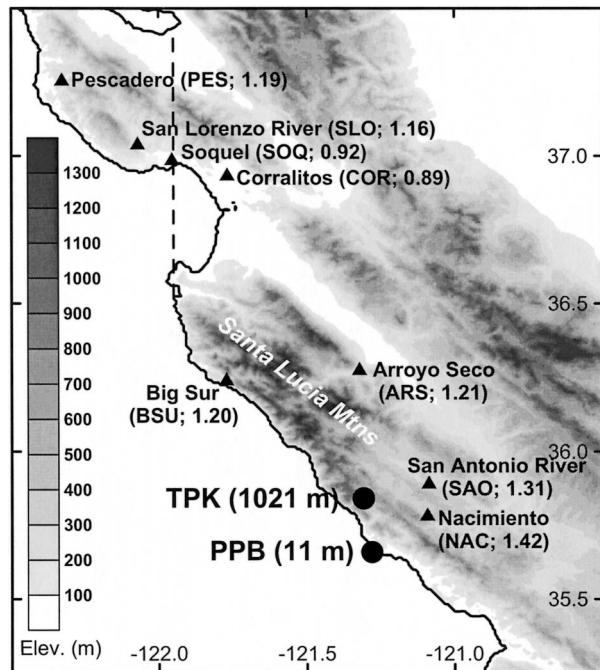The base map (Fig. 9) also shows the location of the

FIG. 9. Terrain base map of central California showing the location of gauging stations (solid triangles, ▲) with recorded annual peak floods. The three-letter station name for each site is included in parentheses, as is the normalized El Niño flood magnitude for $p_e =$ 0.20, that is, a 5-yr flood. The wind profiler and rain gauges at PPB and TPK are depicted by solid circles, and the site elevations are given. The thin dashed line denotes the western edge of the rain shadow created by southerly flow over the Santa Lucia Mountains.
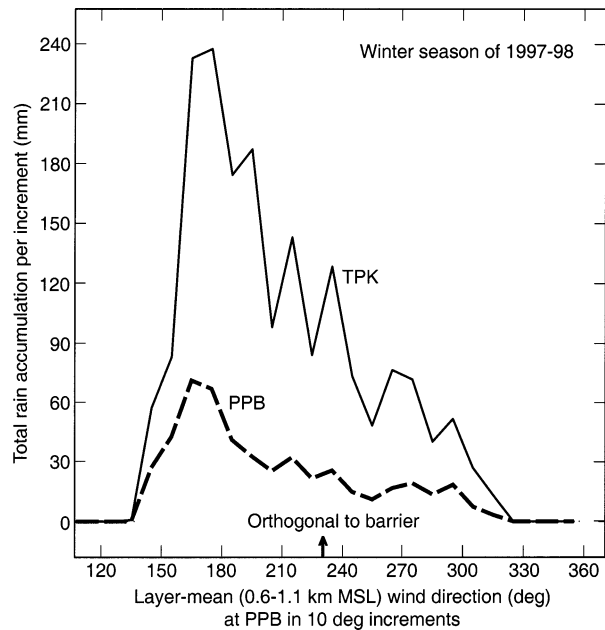

FIG. 10. Layer-mean (0.6–1.1 km MSL), hourly averaged wind direction measured by the PPB wind profiler vs total rainfall at PPB and TPK based on 20 storms during the winter of 1997/98. The rainfall depths were summed over 10° wind-direction increments. The bold arrow extending upward from the bottom frame portrays the flow direction most nearly perpendicular to the mountain barrier.

Point Piedras Blancas (PPB) and Three Peaks (TPK) meteorological sites. The PPB site at the coast contained a 915-MHz wind profiler operated by the National Oceanic and Atmospheric Administration's Environmental Technology Laboratory during the winter of 1997/98 for the California Land-Falling Jets (CALJET) field experiment (Neiman et al. 2002). This profiler provided vertical profiles of horizontal wind from ~0.1 to 4.0 km above ground with 100-m vertical resolution and 1-h temporal resolution in clear, cloudy, and precipitating conditions (e.g., Ecklund et al. 1988). A collocated meteorological tower provided surface data that included tipping-bucket rain gauge measurements. The TPK site in the coastal mountains contained a tipping bucket from California's operational rain gauge network (e.g., Mendell 1992).

During the 1997/98 wet season, November–April, strong El Niño conditions, MEI ≥ 2.2, prevailed. Significant floods occurred at all eight gauging stations during this period, including the largest flood of record at the Pescadero Creek gauge, the second largest flood of record at the San Antonio Creek gauge, and the third largest flood of record at the Big Sur River gauge.

Rainfall recorded at the PPB and TPK meteorological gauges during the winter of 1997/98 are plotted in Fig. 10 versus the prevailing wind direction determined by the PPB profiler at 850 m above ground in 10° increments. The PPB gauge was located near the coast at an elevation 11 m MSL, whereas the TPK gauge was located on a nearby mountainside at an elevation of 1021 m MSL. The substantial differences in total rainfall between the two gauges reflect the large contribution of orographic processes at the mountain gauge. At both meteorological gauges, the greatest rainfall depths accumulated when the wind direction was from the south-southeast to south. In Fig. 9, a light dashed line extending northward from the northwest corner of the Santa Lucia Mountains has been added to indicate the rain shadow of the Santa Lucia Mountains during a storm with prevailing winds from due south. The rain shadow covers the eastern portion of the San Lorenzo River basin, most of the Soquel Creek basin, and all of the Corralitos Creek basin. As the prevailing winds during a storm shift from southerly to southwesterly, the rain shadow decreases over the San Lorenzo, Soquel, and Corralitos basins, because the moist low-level flow reaches these drainage basins directly without first encountering the Santa Lucia Mountains. The Pescadero Creek and Big Sur River basins are not within a rain shadow for storm flow from any direction from south to west, whereas the Arroyo Seco Creek basin is always within the rain shadow of the Santa Lucia Mountains for storm flow from any direction from the south to west.

To further demonstrate the link between the direction of the low-level flow impacting the coastal mountains during El Niño and non–El Niño phases and recorded annual peak floods in the vicinity of the Santa Lucia Mountains, composite analyses of the 925-mb geopotential height (i.e., the low-level geostrophic flow) were constructed using daily global gridded data from the National Centers for Environmental Prediction–National Center for Atmospheric Research reanalysis project (e.g., Kalnay et al. 1996). One composite was created for El Niño conditions (i.e., MEI $\geq$ 0.5) and another for non–El Niño conditions (i.e., MEI < 0.5). For each flood over the entire period of record, 1950–2000, at each of the eight gauging stations shown in Fig. 9, the 24-h-averaged values for the day of the flood and the day preceding the flood were included in the appropriate composite. This approach assumes that the floods were a direct result of heavy rainfall in the coastal mountains and that the heavy rainfall was largely generated by orographic processes. It should be noted that the 925-mb geostrophic wind directions can differ from the actual wind directions along the coast due to a number of factors. Most notably, a terrain-forced ageostrophic barrier jet often develops in response to the deflection or blocking of low-level flow upstream of quasi-two-dimensional mountain ranges (e.g., Parish 1982; Bell and Bosart 1988; Colle and Mass 1995; Overland and Bond 1995; Doyle 1997). This effect would result in flow at $\sim$925 mb that has a larger southerly component than the geostrophic flow. For example, the mean wind direction at $\sim$925 mb recorded by the PPB wind profiler during the rainfall shown in Fig. 10 was 203°, whereas the composite 925-mb geostrophic wind direction for this same time period was 227°.

The composite 925-mb geostrophic wind direction for El Niño floods in the vicinity of the Santa Lucia Mountains was 227°, the same as that observed during the rain events in the winter of 1997/98. In contrast, the composite 925-mb geostrophic wind direction for non–El Niño floods was 241°. Based on the validation described in the previous paragraph, the observed wind flow was quite likely rotated counterclockwise by about 25° relative to the geostrophic flow. The fundamental difference in the composite low-level flow direction for El Niño and non–El Niño phases is consistent with the general observation that storm circulations during developed El Niño conditions tend to be more meridional compared to those during non–El Niño conditions, which tend to be more zonal (e.g., Rasmussen and Wallace 1983; Webb and Betancourt 1992). The composite analysis also provides an explanation for the striking gradient in the relative magnitude of El Niño floods from Pescadero Creek eastward across the San Lorenzo River, Soquel Creek, and Corralitos Creek basins, as well as the anomalously small floods in the Soquel and Corralitos basins during El Niño phases compared to other nearby streams (see Figs. 8a,b). Mean low-level meridional flow conditions that accompany storms during El

Niño conditions impact the Soquel and Corralitos basins only after moisture in this air stream has been depleted by orographic ascent over the Santa Lucia Mountains, whereas mean low-level flows that accompany storms during non–El Niño conditions typically exhibit a larger zonal component that result in a direct fetch from the ocean.

5. Summary and conclusions

The influence of ENSO phase on flooding in California coastal streams was investigated by analyzing the annual peak floods recorded at 38 gauging stations. The multivariate ENSO index (MEI; Wolter and Timlin 1993, 1998), was applied to characterize the ENSO phase at the time of flooding. The best correlations were obtained using the coincident ENSO state, although correlations were nearly as good for many gauging stations using the ENSO state 1–6 months prior to the flood. Previous investigations have demonstrated that monthly and seasonal precipitation and streamflows are moderately well correlated ($r \sim 0.4$–0.6) in southern California. Correlations, however, decrease northward along the coast and disappear north of 37°N. The correlation of log-transformed annual peak floods, log Q_{pk}, with MEI follows a more well-defined south to north trend than previously identified. The magnitude of flooding in all 20 streams located south of 35°N has a significant, positive correlation ($r \sim 0.3$–0.6) with increasing strength of El Niño. Along the central California coast, the correlation of log Q_{pk} with MEI is not statistically significant. Northward from 40°N, the correlation is negative, and in three of the four streams located north of 41°N, flood magnitude has a significant, negative correlation with the MEI.

When the correlation analysis is repeated with the annual peak floods subdivided into those that occurred during El Niño (MEI > 0.5) and non–El Niño (MEI < 0.5) phases, correlation coefficients are uniformly weak and statistically insignificant. The relative strength or development of the El Niño phase has, at most, a weak influence on flood magnitude. A comparison of the geometric mean El Niño flood to the geometric mean non–El Niño flood determined that the means were statistically different at gauging stations south of 35° and north of 41°N. For 20 streams located south of 35°N, the geometric mean of annual peak floods recorded at a stream gauge during El Niño phases is 2 to 14 times the geometric mean of annual peak floods recorded during non–El Niño phases. Thus, south of 35°N along the California coast, floods are significantly larger during an El Niño phase than a non–El Niño phase. For the three streams located north of 41°N, the geometric mean of annual peak floods during an El Niño phase is less than 70% of the geometric mean of annual peak floods during a non–El Niño phase. These results are more indicative of two subsamples of floods, El Niño and

non–El Niño, rather than a linear relation between flood magnitude and MEI.

Flood exceedance probabilities for El Niño and non–El Niño phases were calculated for all 38 gauging station records using a three-parameter log gamma (log–Pearson Type III) distribution. For a given exceedance probability, the ratio of the El Niño to non–El Niño annual peak floods varies from more than 10 near 32°N to less than 0.7 near 42°N. The crossover point where the magnitude of El Niño and non–El Niño floods appear to be nearly identical is in the vicinity of 39°N.

The pattern of increased flood magnitudes in the south and reduced flood magnitudes in the north during developed El Niño conditions is consistent with the observed eastward extension and southward shift of the polar jet. Drainage basin latitude explains 90% of the variation in the relative magnitude of El Niño annual peak floods with an exceedance probability of 0.20 and 76% of the variation in the relative magnitude of El Niño annual peak floods with an exceedance probability of 0.02. Not only is the storm track shifted southward during an El Niño phase, the low-level flow along the California coast becomes less zonal and more meridional, especially during winter storms. A comparison of wind directions along the central California coast shows, on average, a more southerly flow immediately precedes El Niño floods whereas a more southwesterly flow precedes non–El Niño floods. Depending on the upwind topography, this change in wind direction and the corresponding shift in the rain shadow can significantly alter the relative magnitude of El Niño and non–El Niño floods in a given drainage basin. Due to this effect, the relative magnitude of the 0.02 exceedance El Niño flood in Soquel and Corralitos Creeks is approximately half of what would be expected given their location on the California coast.

REFERENCES

Bell, G. D., and L. F. Bosart, 1988: Appalachian cold-air damming. *Mon. Wea. Rev.,* **116,** 137–161.

Cayan, D. R., and D. H. Peterson, 1989: The influence of the North Pacific circulation on streamflow in the West. *Aspects of Climate Variability in the Pacific and Western Americas, Geophys. Monogr.,* No. 55, Amer. Geophys. Union, 375–397.

——, and R. H. Webb, 1992: El Niño/Southern Oscillation and streamflow in the western United States. *Historical and Paleoclimate Aspects of the Southern Oscillation,* H. F. Diaz and V. Markgraf, Eds., Cambridge University Press, 29–68.

——, K. T. Redmond, and L. G. Riddle, 1999: ENSO and hydrologic extremes in the western United States. *J. Climate,* **12,** 2881–2893.

Colle, B. A., and C. F. Mass, 1995: The structure and evolution of cold surges east of the Rocky Mountains. *Mon. Wea. Rev.,* **123,** 2577–2610.

Dettinger, M. D., D. R. Cayan, H. F. Diaz, and D. M. Meko, 1998: North–south precipitation patterns in western North America on interannual-to-decadal timescales. *J. Climate,* **11,** 3095–3111.

——, ——, G. J. McCabe, and J. A. Morego, 2000: Multiscale hydrologic variability associated with El Niño/Southern Oscillation. *El Niño–Southern Oscillation: Multiscale Variability and Societal Impacts,* H. F. Diaz and V. Markgraf, Eds., Cambridge University Press, 114–147.

Doyle, J. D., 1997: The influence of mesoscale orography on a coastal jet and rainband. *Mon. Wea. Rev.,* **125,** 1465–1488.

Dracup, J. A., and E. Kahya, 1994: The relationships between U.S. streamflow and La Niña events. *Water Resour. Res.,* **30,** 2133–2141.

Ecklund, W. L., D. A. Carter, and B. B. Balsley, 1988: A UHF wind profiler for the boundary layer: Brief description and initial results. *J. Atmos. Oceanic Technol.,* **5,** 432–441.

Ely, L. L., Y. Enzel, and D. R. Cayan, 1994: Anomalous North Pacific atmospheric circulation and large winter floods in the southwestern United States. *J. Climate,* **7,** 977–987.

Fu, C., H. F. Diaz, and J. O. Fletcher, 1986: Characteristics of the responses of SST in the central Pacific associated with warm episodes of the Southern Oscillation. *Mon. Wea. Rev.,* **114,** 1716–1738.

Higgins, R. W., J.-K. E. Schemm, W. Shi, and A. Leetmaa, 2000: Extreme precipitation events in the western United States related to tropical forcing. *J. Climate,* **13,** 793–820.

Inman, D. L., and S. A. Jenkins, 1999: Climate change and the episodicity of sediment flux of small California rivers. *J. Geol.,* **107,** 251–270.

Kahya, E., and J. A. Dracup, 1994: The influences of type 1 El Niño and La Niña events on streamflows in the Pacific Southwest of the United States. *J. Climate,* **7,** 965–976.

Kalnay, E., and Coauthors, 1996: The NCEP/NCAR 40-Year Reanalysis Project. *Bull. Amer. Meteor. Soc.,* **77,** 437–471.

Livezey, R. E., M. Masutani, A. Leetmaa, H. Rui, M. Ji, and A. Kumar, 1997: Teleconnective response of the Pacific–North American region atmosphere to large central equatorial Pacific SST anomalies. *J. Climate,* **10,** 1787–1820.

Mendell, T., 1992: Integration of automated hydrological data. Preprints, *ASCE Conf. on Interdisciplinary Approaches in Hydrology and Hydrogeology,* Portland, OR, American Society of Civil Engineers, 7 pp.

Mitchell, T. P., and W. Blier, 1997: The variability of wintertime precipitation in the region of California. *J. Climate,* **10,** 2261–2276.

Neiman, P. J., F. M. Ralph, A. B. White, D. E. Kingsmill, and P. O. G. Persson, 2002: The statistical relationship between upslope flow and rainfall in California's coastal mountains: Observations during CALJET. *Mon. Wea. Rev.,* **130,** 1468–1492.

Overland, J. E., and N. A. Bond, 1995: Observations and scale analysis of coastal wind jets. *Mon. Wea. Rev.,* **123,** 2934–2941.

Parish, T. R., 1982: Barrier winds along the Sierra Nevada Mountains. *J. Appl. Meteor.,* **21,** 921–930.

Rasmusson, E. M., 1985: El Niño and variations in climate. *Amer. Sci.,* **73,** 168–177.

——, and J. M. Wallace, 1983: Meteorological aspects of the El Niño/Southern Oscillation. *Science,* **222,** 1195–1202.

Redmond, K. T., and R. W. Koch, 1991: Surface climate and streamflow variability in the western United States and their relationship to large-scale circulation indices. *Water Resour. Res.,* **27,** 2381–2399.

Ropelewski, C. F., and M. S. Halpert, 1986: North American precipitation and temperature patterns associated with the El Niño/Southern Oscillation (ENSO). *Mon. Wea. Rev.,* **114,** 2352–2362.

Ross, T. F., and J. N. Lott, 2000: A climatology of recent extreme

weather and climate events. National Climatic Data Center Tech. Rep. 2000-02, 9 pp.

Schonher, T., and S. E. Nicholson, 1989: The relationship between California rainfall and ENSO events. *J. Climate,* **2,** 1258–1269.

U.S. Water Resources Council, 1982: Guidelines for determining flood flow frequency. Bulletin 17B, Washington, DC, 183 pp.

Webb, R. H., and J. L. Betancourt, 1992: Climatic variability and flood frequency of the Santa Cruz River, Pima County, Arizona. USGS Water-Supply Paper 2379, 40 pp.

Wolter, K., and M. S. Timlin, 1993: Monitoring ENSO in LOADS with a seasonally adjusted principal component index. *Proc. 17th Climate Diagnostics Workshop,* Norman, OK, NOAA, 52–57.

——, and ——, 1998: Measuring the strength of ENSO events: How does 1997/98 rank? *Weather,* **53,** 315–324.